



Article

Naphthalimide-Modified Tridentate Platinum(II) Complexes: Synthesis, Characterization, and Application in Singlet Oxygen Generation

Zhong-Liang Gong ¹, Qing-Jun Pan ^{1,2}, Dian-Xue Ma ^{1,2} and Yu-Wu Zhong ^{1,2,*}

¹ Beijing National Laboratory for Molecular Sciences, CAS Key Laboratory of Photochemistry, CAS Research/Education Center for Excellence in Molecular Sciences, Institute of Chemistry, Chinese Academy of Sciences, Beijing 100190, China

² School of Chemical Sciences, University of Chinese Academy of Sciences, Beijing 100049, China

* Correspondence: zhongyuwu@iccas.ac.cn

Abstract: Singlet oxygen ($^1\text{O}_2$), representing an important reactive oxygen species, has promising applications in biomedical, material, and environmental sciences. Photosensitized production of $^1\text{O}_2$ using organic dyes is highly desirable and the exploration of highly efficient photosensitizers has received considerable attention. Herein, two tridentate Pt(II) complexes, i.e., cationic **1**(PF₆) and neutral **2**, modified with the ethynynaphthalimide chromophore, were designed and prepared for the application in $^1\text{O}_2$ generation. Spectroscopic studies and computational results suggest that **1**(PF₆) and **2** display the lowest-energy absorption bands centered at 435–465 nm with the molar extinction coefficients of $0.6\text{--}3.2 \times 10^4 \text{ M}^{-1} \text{ cm}^{-1}$, originating from the singlet ligand-to-ligand charge transfer ($^1\text{LLCT}$) and a mixture of $^1\text{LLCT}$ and singlet ligand-centered (LC) transitions, respectively. Moreover, they show similar phosphorescence at 620–640 nm assigned to the Pt-perturbed triplet LC emission of the ethynynaphthalimide moiety. Thanks to the relatively long phosphorescence lifetimes, these complexes exhibit O₂-dependent phosphorescence intensities with good reversibility and stability. They are able to behave as efficient triplet photosensitizers to promote the $^1\text{O}_2$ generation with high quantum yields (84–89%). This work indicates that the combination of an organic chromophore with Pt(II) complexes provides an effective method to obtain photosensitizers for $^1\text{O}_2$ generation.

Keywords: Pt(II) complexes; naphthalimide; photosensitizers; singlet oxygen; energy transfer



Citation: Gong, Z.-L.; Pan, Q.-J.; Ma, D.-X.; Zhong, Y.-W. Naphthalimide-Modified Tridentate Platinum(II) Complexes: Synthesis, Characterization, and Application in Singlet Oxygen Generation. *Inorganics* **2023**, *11*, 438. <https://doi.org/10.3390/inorganics11110438>

Academic Editors: Francis Verpoort, Claudio Pettinari, Maurizio Peruzzini, Richard Layfield, Rainer Winter, Moris S. Eisen, Gábor Papp, Shuang Xiao and Axel Klein

Received: 10 October 2023

Revised: 2 November 2023

Accepted: 15 November 2023

Published: 17 November 2023



Copyright: © 2023 by the authors. Licensee MDPI, Basel, Switzerland. This article is an open access article distributed under the terms and conditions of the Creative Commons Attribution (CC BY) license (<https://creativecommons.org/licenses/by/4.0/>).

1. Introduction

Singlet oxygen ($^1\text{O}_2$), the lowest excited state of the dioxygen molecule, represents an important reactive oxygen species and has attracted great interest in biomedical, material, and environmental sciences due to its extensive applications in photodynamic therapy (PDT), fine chemical synthesis, wastewater treatment, etc. [1–4]. Up until now, a number of chemical and photochemical methods have been developed for the in situ generation of $^1\text{O}_2$. Among them, photosensitized production of $^1\text{O}_2$ using various dyes (also called photosensitizers) is more prevalent [5–7]. As briefly illustrated in Figure 1a, upon photoexcitation, the photosensitizer (PS) is first converted to its lowest singlet excited state (S_1) followed by rapid transition to the lowest triplet excited state (T_1) via fast intersystem crossing (ISC). If effective collision of PS with surrounding O₂ takes place at this moment, the ground triplet-state O₂ ($^3\Sigma_g$) is subsequently excited to generate $^1\text{O}_2$ ($^1\Delta_g$) through energy transfer (EnT) from the T_1 of PS to the $^3\Sigma_g$ state of O₂ [8–10]. For an ideal PS, several characteristics should be met, including strong absorption, high ISC efficiency and long triplet excited-state lifetime (τ_T), good photostability, etc. [11,12].

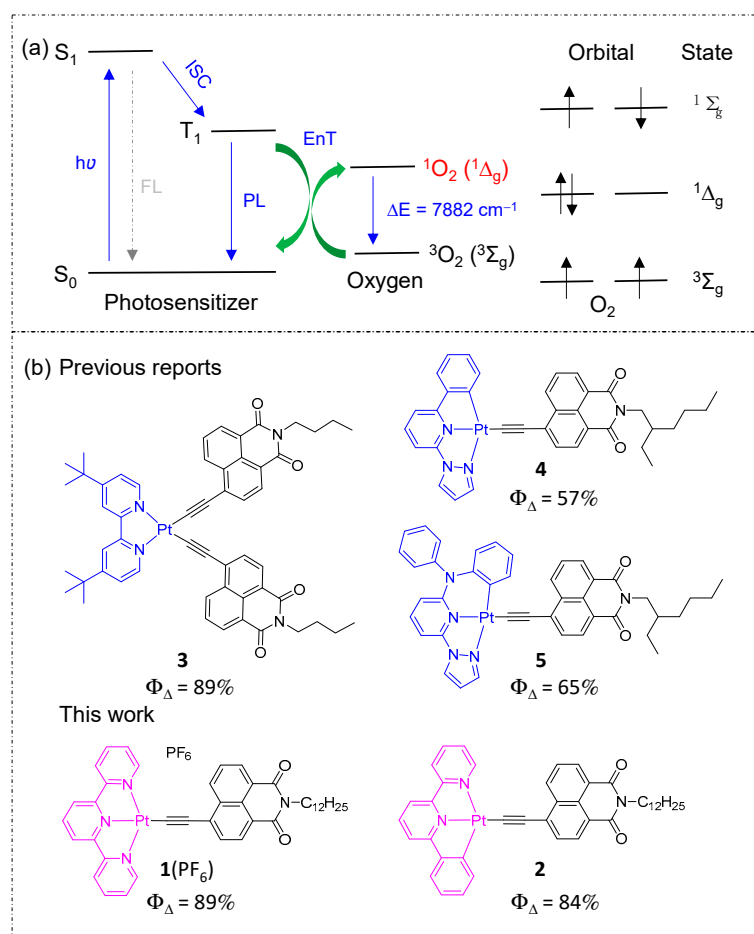


Figure 1. (a) Simplified $^1\text{O}_2$ generation mechanism via energy transfer process from PS to $^3\text{O}_2$ (left) and electronic configurations of the ground state ($^3\Sigma_g$) and first ($^1\Delta_g$) and second ($^1\Sigma_g$) excited states of O_2 (right). ISC: intersystem crossing; EnT: energy transfer; FL: fluorescence; PL: phosphorescence. (b) Previously reported naphthalimide-Pt(II) PSs **3**–**5** (upper) and two analogues, **1**(PF₆) and **2**, studied in this work (lower). The quantum yield for $^1\text{O}_2$ generation in CH₃CN is indicated for each PS.

Over the past few decades, several kinds of classical PSs have been explored and adequately investigated, such as aromatic hydrocarbons, quinones, porphyrins, phthalocyanines, borondipyrromethenes, and transition metal complexes [13–20]. Among them, transition metal complexes, especially Ru(II), Ir(III), Pt(II), and Au(I) complexes, exhibit advantages including large ISC rates benefiting from the strong spin-orbit coupling (SOC), rich coordination modes, and excellent structural modification abilities, endowing them with potential photosensitizing function [21–24]. In view of the larger SOC constant ($\zeta = 4481 \text{ cm}^{-1}$) of the Pt atom relative to other transition metals and the fascinating photophysical properties of related complexes [25–27], Pt(II) complexes become one of the most promising PSs. A certain number of Pt(II) complexes have been reported to display high quantum yields of $^1\text{O}_2$ generation (Φ_Δ). Nonetheless, some drawbacks, e.g., short absorption wavelengths ($\leq 450 \text{ nm}$), low molar absorptivities ($\leq 10^4 \text{ M}^{-1} \text{ cm}^{-1}$), and short triplet excited-state lifetimes, are found in these complexes. Therefore, continuous studies on these complexes to further improve their photosensitizing performances are necessary [28–33].

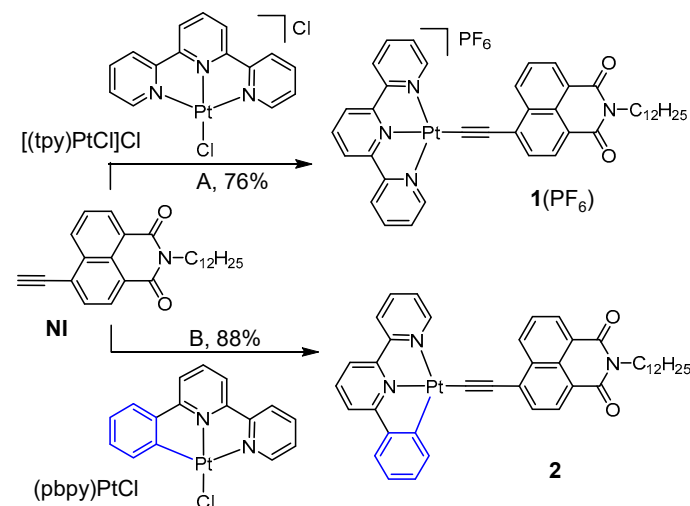
In order to address the issues mentioned above, one straightforward approach is attaching a suitable light-harvesting chromophore with strong absorptivity to the metal component through a π -conjugated bond [11,33–36]. For instance, Zhao and coworkers prepared bidentate (N,N)-Pt(II) complex **3** with two ethynynaphthalimide ligands, displaying a prolonged τ_T of up to 64 μs (in N_2 -saturated solution) and higher Φ_Δ of 89% in

CH₃CN relative to those ($\tau_T = 0.98 \mu\text{s}$; $\Phi_\Delta = 38\%$) of a Pt(II)-ethynylbenzene analogue [35]. Similarly, they reported two tridentate (N⁺N⁺C)- and (N⁺N⁺C)-Pt(II) complexes, **4** and **5**, modified with an ethynyl-naphthalimide ligand to present a moderate Φ_Δ of 57% and 65% in CH₃CN, respectively [36]. Herein, two tridentate Pt(II) complexes, cationic **1**(PF₆) and neutral **2** distinguished by an N⁺N⁺N and cyclometalated N⁺N⁺C coordination mode, respectively, are presented. Both of them contain an appended ethynyl-naphthalimide moiety as an additional chromophore to modulate their photophysical properties. Spectroscopic measurements demonstrate that **1**(PF₆) and **2** show strong visible absorptions extending to ca. 550 nm and improved phosphorescence lifetimes. Meanwhile, their distinct responses to triplet oxygen (³O₂) accompanied by the dramatic decrease in the phosphorescence intensities and highly efficient in situ generation ($\Phi_\Delta = 84\text{--}89\%$) of ¹O₂ via EnT are clearly detected and fully discussed.

2. Results and Discussion

2.1. Synthesis and X-ray Single-Crystal Diffraction Analysis

As outlined in Scheme 1, two Pt(II) complexes, **1**(PF₆) and **2**, were prepared with the one-step ancillary ligand exchange reaction of 2-dodecyl-6-ethynyl-1H-benzo[de]isoquinoline-1,3(2H)-dione (**NI**) with the cationic precursor [(tpy)PtCl]Cl (tpy represents 2,2':6',2''-terpyridine) and the neutral precursor (pbpy)PtCl (pbpy denotes 6-phenyl-2,2'-bipyridine), with the assistance of KOH and a catalytic amount of CuI in a 76% and 88% yield, respectively. Their molecular structures were fully characterized with proton nuclear magnetic resonance (¹H NMR) spectroscopy, high-resolution mass spectrometry (HRMS), and an elemental analysis (details are given in the Section 3). The introduction of the long alkyl chain (*n*-C₁₂H₂₅) into the **NI** ligand and the resulting complexes can significantly improve their solubilities in common organic solvents, and thus facilitate the separation and purification of these materials.



Scheme 1. Synthetic routes to **1**(PF₆) and **2**. Conditions: A. (i) KOH, CH₃OH, 0.5 h; (ii) CuI, [(tpy)PtCl]Cl, rt, overnight; (iii) sat. KPF₆ (aq.). B. (i) KOH, CH₃OH, 0.5 h; (ii) CuI, (pbpy)PtCl, CH₂Cl₂, rt, overnight.

A single crystal of **2** suitable for the X-ray diffraction analysis was successfully obtained with slow diffusion of ethyl ether into the solution of **2** in CH₂Cl₂. The relevant crystallographic data are summarized in Table S1 and the molecular structure and stacking model are shown in Figures 2 and S1. The planar Pt component and the ethynyl-naphthalimide fragment are linked together with a large dihedral angle of ca. 81° via a Pt-C σ -bond with a length of 1.97 Å (Pt1-C70). This means that these two components are almost perpendicular to each other. The Pt-C σ -bond of Pt with the cyclometalating ligand (Pt1-C10) has a slightly longer length of 2.063 Å. The two Pt-N bonds have a length of 2.000 Å (Pt1-N8; with

the middle pyridine of the tridentate ligand) and 2.062 Å (Pt1-N20; with the side pyridine), respectively (Figure 2a). These bond lengths are consistent with those of known tridentate Pt(II)-acetylene analogues [37,38]. Additionally, complex **2** crystallizes in a triclinic $P\bar{1}$ space group with two molecules being included in one unit cell. In the crystal packing, a type of chain-like supramolecular polymer is formed via the alternate π - π stackings of two intermolecular naphthalimide moieties with a distance of 3.47 Å and two cyclometalated Pt components with a distance of 3.305 Å, respectively. No effective metallophilic interaction is present in the crystal structure as the shortest detected intermolecular Pt...Pt distance is about 5.11 Å, which is much longer than the van der Waals contact distance of 3.5 Å of two Pt atoms (Figures 2b and S1).

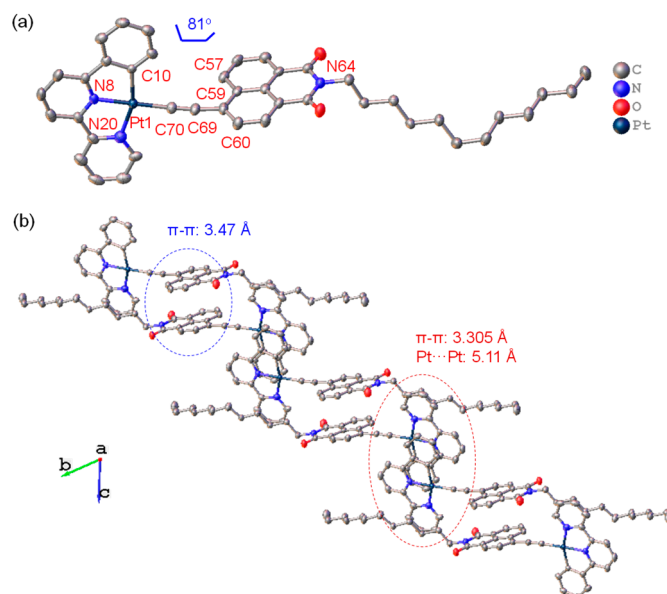


Figure 2. Single-crystal structure of **2** with thermal ellipsoids at 50% probability level. (a) A single molecule viewed from the c axis. (b) A supramolecular polymeric structure formed with alternate π - π stackings of naphthalimide moieties (blue circle) and cyclometalated Pt components (red circle). Hydrogen atoms and counteranions (PF_6^-) are omitted for clarity. Selected bond lengths (Å)—Pt1-N8: 2.000, Pt1-N20: 2.062, Pt1-C10: 2.063, Pt1-C70: 1.970, C70-C69: 1.189, C69-C59: 1.437. Selected bond or torsion angles ($^\circ$)— $\angle\text{N8-Pt1-N20}$: 80.464, $\angle\text{N8-Pt1-C10}$: 79.603, $\angle\text{N8-Pt1-N70}$: 178.384, $\angle\text{N20-Pt1-C10}$: 160.050, $\angle\text{N20-Pt1-C70}$: 100.698, $\angle\text{C10-Pt1-C70}$: 99.215, $\angle\text{Pt1-C70-C69}$: 176.731, $\angle\text{C70-C69-C59}$: 174.449, $\angle\text{N20-N8-C10-Pt1}$: 0.656, $\angle\text{C70-C57-N64-C60}$: 8.915, $\angle\text{C57-C59-Pt1-C10}$: 81.411.

2.2. Steady-State Absorption and Emission Spectroscopies

UV-Vis absorption and steady-state emission properties of **1**(PF_6) and **2** were first investigated in 1,2-dichloroethane (DCE) with a concentration of 5×10^{-5} M (Figure 3 and Table 1). These two complexes display a series of intense absorption bands in the monitored spectral region of 250–600 nm with the molar extinction coefficients (ϵ_{max}) of $0.6\text{--}3.1 \times 10^4$ and $2.0\text{--}4.6 \times 10^4$ $\text{M}^{-1} \text{cm}^{-1}$, respectively (Figure 3a,c). With reference to previous reports [37–40], the high-energy vibronic-structured absorptions of **1**(PF_6) and **2** with the absorption maximum (λ_{abs}) below 380 nm are mainly ascribed to the ligand-centered (^1LC) $^1\pi \rightarrow \pi^*$ transitions of the NI moiety, tpy and pbpy ligands, while the broad absorptions in the range of 380–550 nm can be assigned to an admixture of ^1LC /charge-transfer (^1CT) transitions. In comparison with precursors [(tpy)PtCl]Cl and (pbpy)PtCl, complexes **1**(PF_6) and **2** show red-shifted absorptions with distinctly enhanced molar absorptivities in the lower-energy region, which are also more intense than those of related Pt(II)-phenylacetylide complexes. This reflects the effective electronic interaction between the Pt component and the NI moiety, leading to the appearance of new CT absorptions. The specific assignments with more detailed information will be further discussed later with the aid of time-dependent density functional theory (TD-DFT) calculations.

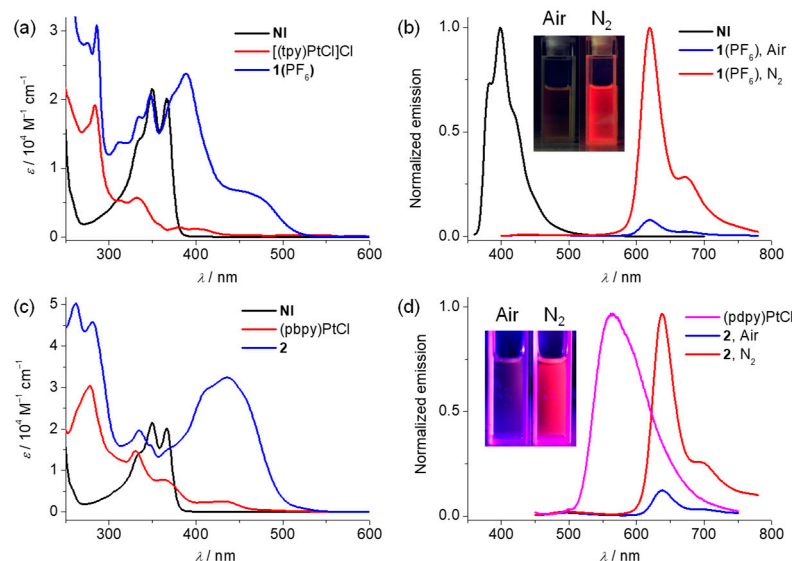


Figure 3. (a,c) UV-Vis absorption and (b,d) steady-state emission of [(tpy)PtCl]Cl (non-emissive), (pbpy)PtCl, NI, 1(PF₆), 2 in air-equilibrated (containing about 21% O₂) or N₂-saturated DCE (5 × 10^{−5} M). Inset: photos of 1(PF₆) and 2 solutions in DCE under air-equilibrated and N₂-saturated conditions upon 365 nm irradiation. Excited at 385 nm for 1(PF₆) and 435 nm for 2 at rt for emission spectra.

Table 1. Photophysical parameters ¹.

Parameter	Compound	1(PF ₆)		2		NI
		DCE	CH ₃ CN	DCE	CH ₃ CN	DCE
λ_{abs} (nm)/ ϵ (10 ⁴ M ^{−1} cm ^{−1})		465/0.6	435/1.3	437/3.2	440/1.7	
		389/2.4	385/2.6	412/2.9	405/1.3	366/2.0
		348/2.1	343/2.1	335/2.0	330/0.9	350/2.2
		286/3.1	282/3.4	282/4.6	279/2.1	
λ_{em} (nm)		620	618	640	636	400
τ (μs) air/N ₂		0.6/4.8	0.27/3.2	0.72/7.0	0.24/1.65	3 × 10 ^{−4} /--
Φ^2 (%) air/N ₂		0.3/1.9	--/0.4	0.3/1.9	0.1/0.9	8.1/--
k_r^3 (10 ³ s ^{−1}) air/N ₂		5.0/4.0	--/1.2	4.2/2.7	4.2/5.4	2.7 × 10 ⁵ /--
k_{nr}^4 (10 ⁵ s ^{−1}) air/N ₂		16.6/2.0	--/3.1	13.8/1.4	41.6/6.0	30.6 × 10 ³ /--
k_q^5 (10 ⁸ M ^{−1} s ^{−1})		9.1	18	7.8	19	--
Φ_{Δ}^6 (%)		--	89	--	84	--
$P_{\text{T},\text{O}_2}^7$ (%)		--	92	--	85	--
$f_{\text{T},\Delta}^8$ (%)		--	97	--	99	--

¹ Monitored in specific solution with the concentration of 5 × 10^{−5} mol L^{−1}. The mark of "--" denotes "No determined". ² Absolute quantum yield. ³ $k_r = \Phi/\tau$. ⁴ $k_{\text{nr}} = (1 - \Phi)/\tau$. ⁵ Phosphorescence quenching rate constant by air (containing about 21% O₂). ⁶ Quantum yield of ¹O₂ generation with respect to that of [Ru(bpy)₃]Cl₂ in CH₃CN ($\Phi_{\Delta} = 57\%$). ⁷ The proportion of triplet excited state of PS quenched with ³O₂. ⁸ The fraction of the triplet state of PS quenched with ³O₂, which leads to ¹O₂ generation.

The NI ligand shows a ¹LC emission band at 400 nm (Figure 3b). Complex (pbpy)PtCl displays a triplet LC (³LC) emission band at 560 nm (Figure 3d) [41], while complex [(tpy)PtCl]Cl is non-emissive at rt [42,43]. In comparison, complexes 1(PF₆) and 2 display a similar lower-energy emission with vibronic characteristics in DCE (5 × 10^{−5} M). Under the air-equilibrated condition, the emission of 1(PF₆) locates at 620 nm with an absolute quantum yield (Φ_{air}) of 0.3% and lifetime (τ_{air}) of 0.6 μs, and the emission of complex 2 is observed at 640 nm with Φ_{air} of 0.3% and τ_{air} of 0.72 μs. Meanwhile, at the N₂-saturated condition, both emissions exhibit a distinct intensity enhancement ($\Phi_{\text{N}_2} = 1.9\%$) and elongated lifetimes with τ_{N_2} of 4.8 and 7.0 μs, respectively (Tables 1 and S2). These properties are superior to those of two Pt(II) precursors and reported Pt(II)-phenylacetylide

analogues [37–39]. The highly O₂-dependent emissions indicate their phosphorescence features. In accordance with the previous works [36,40,44] and TD-DFT calculations, the phosphorescences of **1**(PF₆) and **2** are considered to stem from the Pt-perturbed $^3\pi \rightarrow \pi^*$ (^3LC) transition of the **NI** fragment (see further discussions in following section). Furthermore, benefiting from the long lifetimes of triplet excited states and the good photostability of **1**(PF₆) and **2**, their phosphorescence emissions showed a good reversibility in response to the alternate saturation with N₂ and air (containing about 21% O₂). Under repeated treatment with N₂ and air for eight cycles, the phosphorescence intensity showed no apparent attenuation, indicative of their potentials for O₂ sensing (Figure S2).

Considering that the $^1\text{O}_2$ generation experiment is often measured in CH₃CN [3,9], other than DCE, the comparative study of the spectroscopic properties of **1**(PF₆) and **2** in these two solvents was subsequently conducted (Figure S3). For cationic **1**(PF₆), the lowest energy absorption band displays a distinct hypsochromic shift from 465 nm in DCE to 437 nm in the more polar CH₃CN. The negative solvatochromic effect suggests that the dipole moment of **1**(PF₆) in the ground state is larger with respect to that in the excited state and the ground-state molecules are better stabilized with solvation than the excited-state molecules [44,45]. In contrast, the absorptions of neutral **2** in DCE and CH₃CN display an insignificant spectral change. In a sense, the obvious solvent polarity-dependent absorption spectral shift of **1**(PF₆) points to its more CT-contributed character of the lowest-lying singlet electronic transition relative to that of **2**. Unlike the absorption spectra, the phosphorescence profiles of **1**(PF₆) and **2** almost remain unchanged in these two solvents under air/N₂-saturated conditions, indicative of their dominant ^3LC transition characters as mentioned above.

2.3. Theoretical Calculations

To further elucidate the electronic structures of **1**(PF₆) and **2**, DFT and TD-DFT calculations were carried out. In order to save time and cost, the calculations were performed on the two corresponding model complexes, [**Me-1**]⁺ and **Me-2**, with a methyl group as the substituent on the nitrogen atom of the **NI** fragment. The crystallographic data of **2** were used to build the initial structures for the geometry optimization of [**Me-1**]⁺ and **Me-2** at the ground state (S₀) and the lowest-lying triplet state (T₁). The DFT-optimized structures of **Me-2** and [**Me-1**]⁺ at the ground state show smaller dihedral angles between **NI** and the Pt fragments with respect to that of **2** in the crystal state (Figure S4). The highest occupied molecular orbitals (HOMOs) are mainly related to the ethynynaphthalimide moiety (89% for [**Me-1**]⁺ and 82% for **Me-2**) with a minor contribution of Pt (8.2% for [**Me-1**]⁺ and 13.6% for **Me-2**). The lowest unoccupied molecular orbital (LUMO) of [**Me-1**]⁺ is primarily localized on the tpy fragment (86%) with a minor distribution on Pt (5.6%), but that of **Me-2** has almost equal contributions from pbpy (50%) and **NI** fragments (46%) with a little participation of Pt (4%) (Figure 4c,d). More detailed information on the frontier molecular orbitals of [**Me-1**]⁺ and **Me-2** is displayed in Figures S5 and S6.

In order to obtain insight into the excited state characters of **1**(PF₆) and **2**, TD-DFT calculations were performed for the optimized S₀ structures of **Me-2** and [**Me-1**]⁺, and the predicted vertical excitations from S₀ to various singlet (S_n) excited states are summarized in Table 2. The simulated singlet absorption spectra are shown in Figure 4a,b. The S₀→S₁ excitations were predicted to locate at 470 nm for [**Me-1**]⁺ with an oscillator strength (*f*) of 0.2487 and at 440 nm with *f* of 0.3582 for **Me-2**, respectively. These excitations are in good agreement with the observed lowest-energy absorption maximum of 465 nm for **1**(PF₆) and 437 nm for **2**, respectively. The S₀→S₁ excitations of [**Me-1**]⁺ and **Me-2** are both dominated by the HOMO→LUMO electronic transitions and they can be interpreted as the major ligand-to-ligand charge-transfer ($^1\text{L}_{\text{NI}}\text{L}_{\text{tpy}}$ CT) and mixed $^1\text{LC}_{\text{NI}}/{}^1\text{L}_{\text{NI}}\text{L}_{\text{bpy}}$ CT (bpy stands for the bipyridine segment of the pbpy ligand) transitions, respectively, which are in accordance with the observation of their solvent-dependent absorptions.

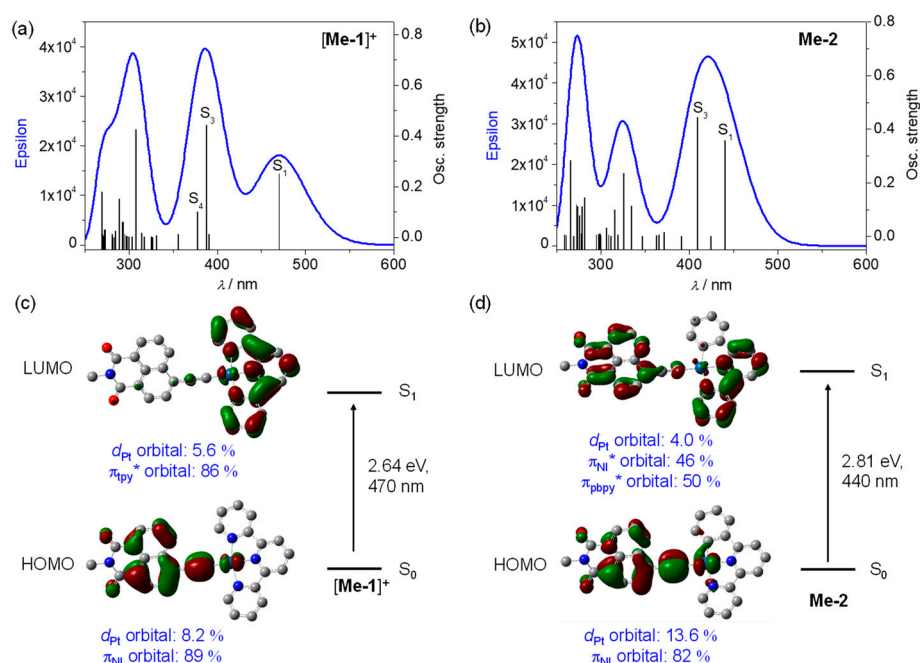


Figure 4. (a,b) TD-DFT-computed singlet vertical excitations (black) and simulated absorption spectra (blue) of (a) [Me-1]⁺ and (b) Me-2. (c,d) Isodensity plots of the major frontier molecular orbitals associated with the S₀→S₁ vertical excitations based on optimized S₀ geometries (isovalue = 0.03) and the energy level diagrams of (c) [Me-1]⁺ and (d) Me-2.

Table 2. Selected TD-DFT-computed singlet vertical excitations from S₀ to S_n states based on optimized S₀ structure ^a.

Complexes	Electronic Transitions	E (eV)	λ (nm)	f	Major Transitions (Percentage)	Characters
[Me-1] ⁺	S ₀ →S ₁	2.64	470	0.2487	HOMO→LUMO (97%)	L _{Ni} L _{tpy} CT/ML _{tpy} CT
	S ₀ →S ₂	3.17	390	0.0114	HOMO→LUMO+1 (97%)	L _{Ni} L _{tpy} CT/ML _{tpy} CT
	S ₀ →S ₃	3.20	388	0.4426	HOMO→LUMO+2 (57%)	LC _{Ni}
					HOMO−1→LUMO (40%)	ML _{tpy} CT/L _{Ni} L _{tpy} CT
	S ₀ →S ₄	3.28	378	0.1013	HOMO−1→LUMO (55%)	ML _{tpy} CT/L _{Ni} L _{tpy} CT
					HOMO→LUMO+2 (41%)	LC _{Ni}
Me-2	S ₀ →S ₁	2.81	440	0.3582	HOMO→LUMO (93%)	LC _{Ni} /L _{Ni} L _{bpy} CT/ML _{bpy} CT
	S ₀ →S ₂	2.92	424	0.0019	HOMO−1→LUMO (71%)	IL _{pbpy} CT/L _{bpy} L _{Ni} CT
					HOMO−1→LUMO+1 (24%)	IL _{pbpy} CT/L _{bpy} L _{Ni} CT
	S ₀ →S ₃	3.03	408	0.4450	HOMO→LUMO+1 (84%)	LC _{Ni} /L _{Ni} L _{bpy} CT/ML _{bpy} CT

^a Calculation method: PBE1PBE/6-311G*/SDD.

Furthermore, the spin density distributions of [Me-1]⁺ and Me-2 were calculated on the optimized T₁ geometries to probe the natures of the phosphorescence of 1(PF₆) and 2 (Figure 5). The results show that the spin densities are mainly distributed on the π-orbitals of the ethynynaphthalimide moiety with a minor involvement of the d-orbital of Pt metal. On the basis of these results, we tentatively assign the low-energy phosphorescence of 1(PF₆) and 2 to the Pt-perturbed ³LC transition of the ethynynaphthalimide segment. This assignment is consistent with the fact that the phosphorescence of complexes 1(PF₆) and 2 involves similar solvent polarity-independent vibronic structures and emission wavelength range.

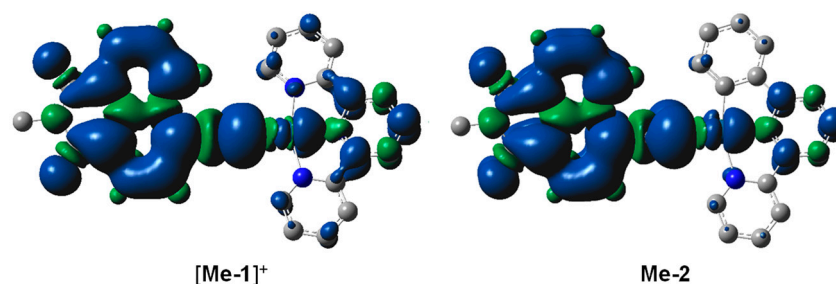


Figure 5. Spin density distributions of $[\text{Me-1}]^+$ and **Me-2** calculated based on optimized T_1 geometries (isovalue = 0.0004).

2.4. Singlet Oxygen Generation

The small triplet radiative transition rate constants (k_r), even at the N_2 -saturated condition, which is $4 \times 10^3 \text{ s}^{-1}$ for **1**(PF_6) and $2.7 \times 10^3 \text{ s}^{-1}$ for **2**, respectively, result in their low Φ_{N_2} of ca. 1.9% (Table 1). Moreover, Φ_{N_2} as well as the average τ are further diminished under the air-equilibrated condition along with the relatively large nonradiative transition rate constants (k_{nr} in the order of 10^6 s^{-1}). The phosphorescence diminishment under the air-equilibrated condition can be rationalized with Equation (1) as a result of the emission quenching with $^3\text{O}_2$ [46].

$$\frac{\tau_{\text{N}_2}}{\tau_{\text{air}}} = \frac{\Phi_{\text{N}_2}}{\Phi_{\text{air}}} = 1 + k_q \tau_{\text{N}_2} [\text{O}_2] \quad (1)$$

wherein $[\text{O}_2]$ represents the concentration of $^3\text{O}_2$ and is taken as $1.6 \times 10^{-3} \text{ M}$ in air-equilibrated DCE at rt [47] and τ_{N_2} and τ_{air} are phosphorescence lifetimes under N_2 -saturated and air-equilibrated conditions, respectively. On the basis of Equation (1), the phosphorescence quenching rate constants (k_q) were calculated to be ca. 9.1 and $7.8 \times 10^8 \text{ M}^{-1} \text{ s}^{-1}$ for **1**(PF_6) and **2**, respectively, which are comparable with those of other known Pt analogues [28,48]. These k_q values are around 1/9 of the diffusion-controlled rate constant (k_{diff}), given that k_{diff} is taken to be $8.5 \times 10^9 \text{ M}^{-1} \text{ s}^{-1}$ in DCE at rt. This suggests that the phosphorescences of **1**(PF_6) and **2** are quenched with $^3\text{O}_2$ exclusively through an EnT process [49]. The similar EnT phosphorescence quenching processes with $^3\text{O}_2$ are also believed to take place in CH_3CN ($[^3\text{O}_2] = 1.9 \times 10^{-3} \text{ M}$) as the k_q of **1**(PF_6) and **2** in CH_3CN (1.8 and $1.9 \times 10^9 \text{ M}^{-1} \text{ s}^{-1}$, respectively) are also around 1/9 of corresponding k_{diff} ($1.9 \times 10^{10} \text{ M}^{-1} \text{ s}^{-1}$). In addition, the excited-state energies of the T_1 state ($E_{\text{T1},00}$) of **1**(PF_6) and **2** were calculated with $E_{\text{T1},00} = 1240/\lambda_{\text{emi}}$ to be ca. 2.0 and 1.9 eV, respectively, both of which are larger than the first ($^1\Delta_g$) and second ($^1\Sigma_g$) excited-state energies of $^1\text{O}_2$ (ca. 1.6 and 1.0 eV, respectively) in non-aqueous solvents [50–52]. This suggests that the EnT processes from **1**(PF_6) and **2** to $^3\text{O}_2$ are exothermic, leading to the effective generation of $^1\text{O}_2$.

The generation of $^1\text{O}_2$ was further quantified by integrating the NIR emission of $^1\text{O}_2$ at 1270 nm in air-equilibrated CH_3CN of **1**(PF_6) and **2** in comparison with that of $[\text{Ru}(\text{bpy})_3]\text{Cl}_2$ as the reference compound (Figures 6 and S7). By plotting the emission integrals of $^1\text{O}_2$ (I_{O_2}) as a function of the absorbances (A) at the excitation wavelength of 435 nm in a series of solutions of these compounds with variable concentrations, three linearly fitted curves with different slopes, $S(I_{\text{O}_2}/A)$, are obtained (Figure 6b). The quantum yields of the $^1\text{O}_2$ generation of **1**(PF_6) and **2** were thus estimated to be 89% and 84%, respectively, according to Equation (2), in which $\Phi_{\Delta,\text{ref}}$, $I_{\text{O}_2,\text{ref}}$, A_{ref} , and $S(I_{\text{O}_2,\text{ref}}/A_{\text{ref}})$ are the various parameters of the reference standard $[\text{Ru}(\text{bpy})_3]\text{Cl}_2$ ($\Phi_{\Delta} = 57\%$ in CH_3CN) [49,50]. The determined Φ_{Δ} of these complexes are comparable with or even higher than those of known tridentate Pt(II)-arylacetylide analogues [36,53–55].

$$\frac{\Phi_{\Delta}}{\Phi_{\Delta,\text{ref}}} = \frac{I_{\text{O}_2} \times A_{\text{ref}}}{I_{\text{O}_2,\text{ref}} \times A} = \frac{S(I_{\text{O}_2}/A)}{S(I_{\text{O}_2,\text{ref}}/A_{\text{ref}})} \quad (2)$$

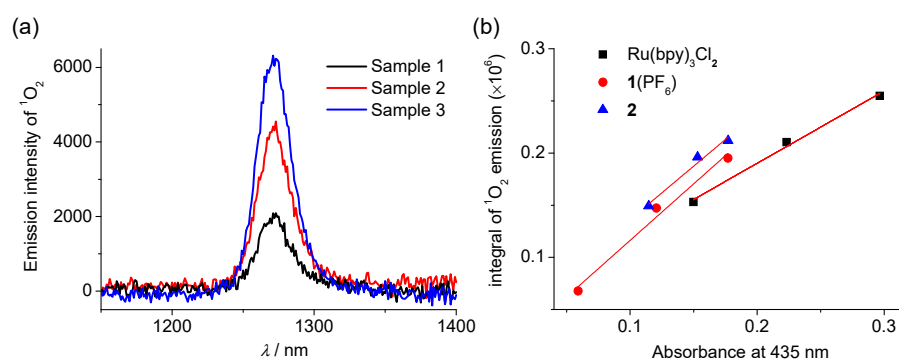


Figure 6. (a) Near-infrared (NIR) emission spectra of $^1\text{O}_2$ in air-equilibrated CH_3CN containing $1(\text{PF}_6)$ with different concentrations (sample 1–3) under excitation at 435 nm. (b) The plots and linearly fitted curves of the integral $^1\text{O}_2$ emission at 1270 nm versus the absorbance at 435 nm of $1(\text{PF}_6)$ (red), **2** (blue), and $[\text{Ru}(\text{bpy})_3]\text{Cl}_2$ (black) in air-equilibrated CH_3CN .

The good linear correlation between the integral of the $^1\text{O}_2$ emission intensity and the absorbance at the excitation wavelength indicates that the triplet–triplet annihilation in these diluted solutions is negligible. Furthermore, Φ_Δ can be expressed with Equation (3):

$$\Phi_\Delta = \Phi_T P_{T,\text{O}_2} f_{T,\Delta} \quad (3)$$

wherein Φ_T is the efficiency of triplet formation and estimated to be unity for $1(\text{PF}_6)$ and **2** in view of the strong SOC of the heavy Pt atom. In addition, P_{T,O_2} refers to the proportion of the triplet excited state quenched with $^3\text{O}_2$ and can be estimated to be 92% and 85% for $1(\text{PF}_6)$ and **2**, respectively, with Equation (4).

$$P_{T,\text{O}_2} = 1 - (\tau_{\text{Air}} / \tau_{\text{N}_2}) \quad (4)$$

The values of $f_{T,\Delta}$ in Equation (3), standing for the fraction of the triplet state quenched with $^3\text{O}_2$, which leads to the generation of $^1\text{O}_2$, are calculated to be ca. 97% and 99% for $1(\text{PF}_6)$ and **2**, respectively.

3. Experimental Section

3.1. General Information for Synthesis and Characterization

A Bruker Advance 400 MHz spectrometer was employed to measure the ^1H NMR spectra in the designated solvents. The ^1H NMR data are reported in ppm with respect to the residual protons of deuterated solvents. An Autoflex III matrix-assisted laser desorption ionization time-of-flight (MALDI-TOF) mass spectrometer was used to measure the high-resolution mass spectra. The elemental analysis was obtained on a Flash EA 1112 or Carlo Erba 1106 analyzer. Ligand **NI** and the precursor complexes $[(\text{tpy})\text{PtCl}]\text{Cl}$ and $(\text{pdpy})\text{PtCl}$ were prepared according to the previous reports [56,57].

Synthesis of $1(\text{PF}_6)$. Into a round-bottom flask containing the **NI** ligand (214 mg, 0.55 mmol, 1.1 equiv) and KOH (56 mg, 1.0 mmol, 2.0 equiv), 20 mL of CH_3OH was injected under a N_2 atmosphere. The obtained mixture was stirred at rt for 0.5 h. After that, $[(\text{tpy})\text{PtCl}]\text{Cl}$ (250 mg, 0.50 mmol, 1.0 equiv) and CuI (57 mg, 0.30 mmol, 0.60 equiv) were added and the mixture was bubbled with N_2 for 10 min. After stirring at rt overnight, the mixture was concentrated, followed by the addition of the proper amount of ethyl ether. The appeared precipitate was collected using filtration. The obtained solid was then dispersed in 20 mL of CH_3OH , followed by the addition of 20 mL of a saturated aq. KPF_6 solution. After stirring for an additional 3 h at rt, the precipitate was collected using filtration, and washed with H_2O , ethyl ether, and CH_2Cl_2 successively to give 210 mg of $1(\text{PF}_6)$ as a red solid in a 76% yield. ^1H NMR (400 MHz, $\text{DMSO}-d_6$): δ 9.15 (t, $J = 4.8$ Hz, 2H), 8.80 (t, $J = 8.4$ Hz, 1H), 8.50–8.70 (m, 5H), 8.47–8.53 (m, 3H), 8.38 (t, $J = 7.6$ Hz, 1H), 7.88–7.97 (m, 4H), 4.03 (t, $J = 7.6$ Hz, 2H), 1.64 (t, $J = 7.6$ Hz, 2H), 1.23–1.33 (m, 18H), 0.85 (t,

$J = 6.8$ Hz, 3H). MALDI-HRMS calcd for $[M - PF_6]^+ C_{41}H_{41}N_4O_2Pt$: 816.2877. Found: 816.2875. Anal. Calcd for $C_{41}H_{41}F_6N_4O_2PPt \cdot H_2O$: C, 50.26; H, 4.42; N, 5.72. Found: C, 50.43; H, 4.26; N, 5.70.

Synthesis of 2. Into a round-bottom flask containing the NI ligand (107 mg, 0.28 mmol, 1.1 equiv) and KOH (28 mg, 0.5 mmol, 2.0 equiv), 20 mL of CH_3OH was added under a N_2 atmosphere. The resulting mixture was stirred at rt for 0.5 h. After that, 20 mL of CH_2Cl_2 was injected, followed by the addition of (pbpy)PtCl (115 mg, 0.25 mmol, 1.0 equiv) and CuI (29 mg, 0.15 mmol, 0.60 equiv). The mixture was then bubbled with N_2 for 10 min, and stirred at rt overnight. Into the reaction system, 50 mL of H_2O was added and the mixture was extracted with CH_2Cl_2 (40 mL \times 3). The obtained organic phase was combined. The crude product was purified with flash column chromatography on silica gel (eluent: CH_2Cl_2) to afford 167 mg of **2** as an orange solid in a 88% yield. 1H NMR (400 MHz, $CDCl_3$): δ 9.26 (d, $J = 5.2$ Hz, 1H), 9.09 (dd, $J = 8.4, 1.2$ Hz, 1H), 8.59 (dd, $J = 7.2, 1.2$ Hz, 1H), 8.52 (dd, $J = 8.0$ Hz, 1H), 8.09 (td, $J = 7.6, 1.6$ Hz, 1H), 8.86–8.99 (m, 4H), 7.72 (dd, $J = 8.0, 7.2$ Hz, 1H), 7.65 (dd, $J = 8.0, 1.2$ Hz, 2H), 7.60 (dd, $J = 7.6, 5.2$ Hz, 1H), 7.43 (dd, $J = 7.6, 1.2$ Hz, 1H), 7.20 (td, $J = 7.2, 1.2$ Hz, 1H), 7.11 (td, $J = 7.6, 1.2$ Hz, 1H), 4.18 (t, $J = 7.6$ Hz, 2H), 1.71–1.79 (m, 2H), 1.26–1.45 (m, 18H), 0.88 (t, $J = 6.8$ Hz, 3H). MALDI-HRMS calcd for $[M + H]^+ C_{42}H_{42}N_3O_2Pt$: 815.2925. Found: 815.2924. Anal. Calcd for $C_{42}H_{41}N_3O_2Pt$: C, 61.91; H, 5.07; N, 5.16. Found: C, 61.59; H, 5.05; N, 5.09.

3.2. Information on Other Physical Measurements

A TU-1810DSPC spectrometer of Beijing Purkinje General Instrument Co., Ltd., Beijing, China., was used to measure the absorption spectra at rt. An F-380 spectrofluorimeter of Tianjin Gang-dong Sci. & Tech. Development Co., Ltd., Tianjing, China., was used to measure the luminescence spectra. The excited-state lifetimes were obtained on Quantaaurus-Tau Fluorescence lifetime spectrometer C11367 of Hamamatsu Photonics. The absolute emission quantum yields were determined on Hamamatsu Quantaaurus-QY spectrometer C11347. Near-infrared 1O_2 emission spectra were recorded on an FLS980 spectrometer from Edinburgh Instruments Co., Ltd. equipped with an NIR photomultiplier tube (NIR-PMT, R5509) from Hamamatsu Corporation using excitation at 435 nm with a Xe lamp.

X-ray single-crystal crystallography. A Rigaku Saturn 724 diffractometer was employed to obtain the X-ray diffraction data on a rotating anode (Mo $K\alpha$ radiation, 0.71073 Å) at 173 K. The structure was analyzed using the direct method with SHELXS-9758 and refined on Olex 2.59. Crystallographic data are summarized in Table S1.

DFT and TD-DFT calculations. The Gaussian 09 package was employed for the DFT and TD-DFT calculations with the PBE1PBE exchange correlation functional [58]. The SDD basis set was used for Pt and 6-311G* for other atoms [26]. For all calculations, the solvent effect of 1,2-dichloroethane was taken into account using the self-consistent reaction field (SCRF) and solvent model based on density (SMD) [59].

4. Conclusions

In conclusion, two tridentate Pt(II) complexes, i.e., cationic **1**(PF₆) and neutral **2**, modified with an ethynynaphthalimide chromophore, were successfully synthesized and characterized. These complexes possess strong UV-Vis absorptions and vibronically structured phosphorescence emissions at 620–640 nm in nonpolar DCE and polar CH_3CN . Theoretical calculations suggest that the lowest-energy absorption bands of **1**(PF₆) and **2** are mainly associated with the $^1L_{NI}L_{tpy}CT$ and mixed $^1LC_{NI}/^1L_{NI}L_{bpy}CT$ transitions, respectively, while their low-energy phosphorescences are both associated with the 3LC transition of the ethynynaphthalimide moiety. Benefiting from the long lifetimes of phosphorescence, these two complexes exhibit highly sensitive and reversible responses to O_2 with the high-yield generation (84–89%) of 1O_2 via an EnT process. Thus, these complexes have potential for O_2 sensing and PDT in the future.

Supplementary Materials: The following supporting information can be downloaded at: <https://www.mdpi.com/article/10.3390/inorganics11110438/s1>, Table S1: Crystallographic data of **2**; Table S2: Detailed lifetime data; Figure S1: Molecular dimer in one unit cell and the stacking model of **2**; Figure S2: Responsibility of phosphorescence intensity of **1**(PF₆) and **2** upon repeated exposure of N₂ and air; Figure S3: Solvent effect of absorption and emission for **1**(PF₆) and **2**; Figure S4: Single-crystal structure of **2** and optimized structures of [Me-1]⁺ and Me-2 at ground state; Figures S5 and S6: Isodensity plots of frontier molecular orbitals (MOs) of [Me-1]⁺ and Me-2, respectively; Figure S7: Absorption and NIR emission of ¹O₂ generated with photosensitization of **1**(PF₆) and **2** and reference [Ru(bpy)₃]²⁺ in CH₃CN with different diluted concentrations; Figures S8–S11: ¹H NMR and MS spectra of **1**(PF₆) and **2**; Data S1: cartesian coordinates of DFT-optimized S₀ and T₁ structure of [Me-1]⁺ and Me-2.

Author Contributions: Conceptualization, Y.-W.Z. and Z.-L.G.; methodology, Z.-L.G.; software, Z.-L.G.; validation, Y.-W.Z.; formal analysis, Z.-L.G. and Y.-W.Z.; investigation, Z.-L.G., Q.-J.P., and D.-X.M.; resources, Z.-L.G.; data curation, Z.-L.G.; writing—original draft preparation, Z.-L.G.; writing—review and editing, Y.-W.Z.; visualization, Z.-L.G. and Y.-W.Z.; supervision, Y.-W.Z.; project administration, Y.-W.Z.; funding acquisition, Y.-W.Z. All authors have read and agreed to the published version of the manuscript.

Funding: This research was funded by the National Natural Science Foundation of China, grant numbers: 21925112, 22090021, and 21872154.

Data Availability Statement: Supplementary crystallographic data (CCDC 2206904) can be obtained free of charge from the Cambridge Crystallographic Data Centre via www.ccdc.cam.ac.uk/data_request/cif.

Conflicts of Interest: The authors declare no conflict of interest. The funder had no role in the design of the study; in the collection, analyses, or interpretation of data; in the writing of the manuscript; or in the decision to publish the results.

References

- McKenzie, L.K.; Bryant, H.E.; Weinstein, J.A. Transition metal complexes as photosensitisers in one- and two-photon photodynamic therapy. *Coord. Chem. Rev.* **2019**, *379*, 2–29. [\[CrossRef\]](#)
- DeRosa, M.C.; Crutchley, R.J. Photosensitized singlet oxygen and its applications. *Coord. Chem. Rev.* **2002**, *233–234*, 351–371. [\[CrossRef\]](#)
- Ashen-Garry, D.; Selke, M. Singlet Oxygen Generation by Cyclometalated Complexes and Applications. *Photochem. Photobiol.* **2014**, *90*, 257–274. [\[CrossRef\]](#) [\[PubMed\]](#)
- Li, G.; Wu, M.; Xu, Y.; Wang, Q.; Liu, J.; Zhou, X.; Ji, H.; Tang, Q.; Gu, X.; Liu, S.; et al. Dual-Phosphorescent Iridium(III) Complexes Extending Oxygen Sensing from Hypoxia to Hyperoxia. *Coord. Chem. Rev.* **2023**, *478*, 214979–214998. [\[CrossRef\]](#)
- Redmond, R.W.; Kochevar, I.E. Spatially Resolved Cellular Responses to Singlet Oxygen. *Photochem. Photobiol.* **2006**, *82*, 1178–1186. [\[CrossRef\]](#) [\[PubMed\]](#)
- Schlachter, A.; Asselin, P.; Harvey, P.D. Porphyrin-Containing MOFs and COFs as Heterogeneous Photosensitizers for Singlet Oxygen-Based Antimicrobial Nanodevices. *ACS Appl. Mater. Interfaces* **2021**, *13*, 26651–26672. [\[CrossRef\]](#)
- Younis, M.R.; He, G.; Qu, J.; Lin, J.; Huang, P.; Xia, X.-H. Inorganic Nanomaterials with Intrinsic Singlet Oxygen Generation for Photodynamic Therapy. *Adv. Sci.* **2021**, *8*, 2102587. [\[CrossRef\]](#)
- Schweitzer, C.; Schmidt, R. Physical Mechanisms of Generation and Deactivation of Singlet Oxygen. *Chem. Rev.* **2003**, *103*, 1685–1757. [\[CrossRef\]](#)
- Jiang, X.; Zhu, N.; Zhao, D.; Ma, Y. New cyclometalated transition-metal based photosensitizers for singlet oxygen generation and photodynamic therapy. *Sci. China Chem.* **2016**, *59*, 40–52. [\[CrossRef\]](#)
- Ishii, K. Functional singlet oxygen generators based on phthalocyanines. *Coord. Chem. Rev.* **2012**, *256*, 1556–1568. [\[CrossRef\]](#)
- Zhao, J.; Wu, W.; Sun, J.; Guo, S. Triplet photosensitizers: From molecular design to applications. *Chem. Soc. Rev.* **2013**, *42*, 5323–5351. [\[CrossRef\]](#) [\[PubMed\]](#)
- Zhao, X.; Liu, J.; Fan, J.; Chao, H.; Peng, X. Recent progress in photosensitizers for overcoming the challenges of photodynamic therapy: From molecular design to application. *Chem. Soc. Rev.* **2021**, *50*, 4185–4219. [\[CrossRef\]](#) [\[PubMed\]](#)
- Zhao, J.; Xu, K.; Yang, W.; Wang, Z.; Zhong, F. The triplet excited state of Bodipy: Formation, modulation and application. *Chem. Soc. Rev.* **2015**, *44*, 8904–8939. [\[CrossRef\]](#) [\[PubMed\]](#)
- Langa, K.; Mosinger, J.; Wagnerová, D.M. Photophysical properties of porphyrinoid sensitizers non-covalently bound to host molecules; models for photodynamic therapy. *Coord. Chem. Rev.* **2004**, *248*, 321–350. [\[CrossRef\]](#)
- Pham, T.C.; Nguyen, V.-N.; Choi, Y.; Lee, S.; Yoon, J. Recent Strategies to Develop Innovative Photosensitizers for Enhanced Photodynamic Therapy. *Chem. Rev.* **2021**, *121*, 13454–13619. [\[CrossRef\]](#) [\[PubMed\]](#)

16. Mahammed, A.; Gross, Z. Corroles as triplet photosensitizers. *Coord. Chem. Rev.* **2019**, *379*, 121–132. [\[CrossRef\]](#)
17. Kar, B.; Das, U.; Roy, N.; Paira, P. Recent advances on organelle specific Ru(II)/Ir(III)/Re(I) based complexes for photodynamic therapy. *Coord. Chem. Rev.* **2023**, *474*, 214860–214936. [\[CrossRef\]](#)
18. Xu, Y.; Li, C.; An, J.; Ma, X.; Yang, J.; Luo, L.; Deng, Y.; Kim, J.S.; Sun, Y. Construction of a 980 nm laser-activated Pt(II) metallacycle nanosystem for efficient and safe photo-induced bacteria sterilization. *Sci. China Chem.* **2023**, *66*, 155–163. [\[CrossRef\]](#)
19. Chen, H.; Wen, K.; Lu, Y.; Zhang, X.; Shi, Y.; Shi, Q.; Ma, H.; Peng, Q.; Huang, H. White-light-driven fluorescence switch for super-resolution imaging guided photodynamic and photoacid therapy. *Sci. China Chem.* **2022**, *65*, 2528–2537. [\[CrossRef\]](#)
20. Tian, S.; Lu, Y.; He, Z.; Yue, Q.; Zhuang, Z.; Wang, Y.; Meng, F.; Luo, L. Polydiacetylene-based poly-ion complex enabling aggregation-induced emission and photodynamic therapy dual turn-on for on-demand pathogenic bacteria elimination. *Sci. China Chem.* **2022**, *65*, 1782–1790. [\[CrossRef\]](#)
21. Chen, Y.; Guan, R.; Zhang, C.; Huang, J.; Ji, L.; Chao, H. Two-photon luminescent metal complexes for bioimaging and cancer phototherapy. *Coord. Chem. Rev.* **2016**, *310*, 16–40. [\[CrossRef\]](#)
22. Stacey, O.J.; Pope, S.J.A. New avenues in the design and potential application of metal complexes for photodynamic therapy. *RSC Adv.* **2013**, *3*, 25550–25564. [\[CrossRef\]](#)
23. Ruggi, A.; van Leeuwen, F.W.B.; Velders, A.H. Interaction of dioxygen with the electronic excited state of Ir(III) and Ru(II) complexes: Principles and biomedical applications. *Coord. Chem. Rev.* **2011**, *255*, 2542–2554. [\[CrossRef\]](#)
24. Zhong, Y.-W. Photofunction-Directed Coordination Molecular Engineering. *Chin. J. Chem.* **2021**, *39*, 543–549. [\[CrossRef\]](#)
25. Yam, V.W.-W.; Au, V.K.-M.; Leung, S.Y.-L. Light-Emitting Self-Assembled Materials Based on d⁸ and d¹⁰ Transition Metal Complexes. *Chem. Rev.* **2015**, *115*, 7589–7728. [\[CrossRef\]](#) [\[PubMed\]](#)
26. Gong, Z.-L.; Tang, K.; Zhong, Y.-W. A Carbazole-Bridged Biscyclometalated Diplatinum Complex: Synthesis, Characterization, and Dual-Mode Aggregation-Enhanced Phosphorescence. *Inorg. Chem.* **2021**, *60*, 6607–6615. [\[CrossRef\]](#)
27. Gong, Z.-L.; Zhong, Y.-W.; Yao, J. Regulation of intra- and intermolecular Pt–Pt and π – π interactions of a U-shaped diplatinum complex to achieve pseudo-polymorphic emissions in solution and crystalline states. *J. Mater. Chem. C* **2017**, *5*, 7222–7229. [\[CrossRef\]](#)
28. Djurovich, P.I.; Murphy, D.; Thompson, M.E.; Hernandez, B.; Gao, R.; Hunt, P.L.; Selke, M. Cyclometalated iridium and platinum complexes as singlet oxygen photosensitizers: Quantum yields, quenching rates and correlation with electronic structures. *Dalton Trans.* **2007**, 3763–3770. [\[CrossRef\]](#)
29. Shavaleev, N.M.; Adams, H.; Best, J.; Edge, R.; Navaratnam, S.; Weinstein, J.A. Deep-Red Luminescence and Efficient Singlet Oxygen Generation by Cyclometalated Platinum(II) Complexes with 8-Hydroxyquinolines and Quinoline-8-thiol. *Inorg. Chem.* **2006**, *45*, 9410–9415. [\[CrossRef\]](#)
30. Wu, W.; Yang, P.; Ma, L.; Lalevée, J.; Zhao, J. Visible-Light Harvesting Pt(II) Complexes as Singlet Oxygen Photosensitizers for Photooxidation of 1,5-Dihydroxynaphthalene. *Eur. J. Inorg. Chem.* **2013**, *2013*, 228–231. [\[CrossRef\]](#)
31. Potocny, A.M.; Pistner, A.J.; Yap, G.P.A.; Rosenthal, J. Electrochemical, Spectroscopic, and ¹O₂ Sensitization Characteristics of Synthetically Accessible Linear Tetrapyrrole Complexes of Palladium and Platinum. *Inorg. Chem.* **2017**, *56*, 12703–12711. [\[CrossRef\]](#) [\[PubMed\]](#)
32. Shafikov, M.Z.; Suleymanova, A.F.; Kutta, R.J.; Gorski, A.; Kowalczyk, A.; Gapin'ska, M.; Kowalski, K.; Czerwieniec, R. Ligand design and nuclearity variation towards dual emissive Pt(II) complexes for singlet oxygen generation, dual channel bioimaging, and theranostics. *J. Mater. Chem. C* **2022**, *10*, 5636–5647. [\[CrossRef\]](#)
33. Garai, A.; Villa, M.; Marchini, M.; Patra, S.K.; Pain, T.; Mondal, S.; Ceroni, P.; Kar, S. Synthesis, Structure, Photophysics, and Singlet Oxygen Sensitization by a Platinum(II) Complex of Meso-Tetra-Acenaphthyl Porphyrin. *Eur. J. Inorg. Chem.* **2021**, *2021*, 4089–4095. [\[CrossRef\]](#)
34. Subedi, D.R.; Reid, R.; D'Souza, P.F.; Nesterov, V.N.; D'Souza, F. Singlet Oxygen Generation in Peripherally Modified Platinum and Palladium Porphyrins: Effect of Triplet Excited State Lifetimes and meso-Substituents on ¹O₂ Quantum Yields. *ChemPlusChem* **2022**, *87*, e202200010. [\[CrossRef\]](#) [\[PubMed\]](#)
35. Zhong, F.; Zhao, J.; Hayvali, M.; Elmali, A.; Karatay, A. Effect of Molecule Conformation Restriction on the Photophysical Properties of N^{*}N^{*} Platinum(II) Bis(ethynyl)naphthalimide Complexes Showing Close-Lying ³MLCT and ³LE Excited States. *Inorg. Chem.* **2019**, *58*, 1850–1861. [\[CrossRef\]](#)
36. Wu, W.; Wu, X.; Zhao, J.; Wu, M. Synergetic effect of C^{*}N^{*}N/C^{*}N^{*}N coordination and the arylacetylide ligands on the photophysical properties of cyclometalated platinum complexes. *J. Mater. Chem. C* **2015**, *3*, 2291–2301. [\[CrossRef\]](#)
37. Lu, W.; Mi, B.-X.; Chan, M.C.W.; Hui, Z.; Che, C.-M.; Zhu, N.; Lee, S.-T. Light-Emitting Tridentate Cyclometalated Platinum(II) Complexes Containing σ -Alkynyl Auxiliaries: Tuning of Photo- and Electrophosphorescence. *J. Am. Chem. Soc.* **2004**, *126*, 4958–4971. [\[CrossRef\]](#)
38. Schneider, J.; Du, P.; Jarosz, P.; Lazarides, T.; Wang, X.; Brennessel, W.W.; Eisenberg, R. Cyclometalated 6-Phenyl-2,2'-bipyridyl (CNN) Platinum(II) Acetylide Complexes: Structure, Electrochemistry, Photophysics, and Oxidative and Reductive-Quenching Studies. *Inorg. Chem.* **2009**, *48*, 4306–4316. [\[CrossRef\]](#)
39. Wang, X.; Goeb, S.; Ji, Z.; Castellano, F.N. Excited State Absorption Properties of Pt(II) Terpyridyl Complexes Bearing π -Conjugated Arylacetylides. *J. Phys. Chem. B* **2010**, *114*, 14440–14449. [\[CrossRef\]](#)
40. Zhao, T.; Liu, R.; Shi, H.; Shu, M.; Hu, J.; Li, H.; Zhu, H. Synthesis, tunable photophysics and nonlinear absorption of terpyridyl Pt(II) complexes bearing different acetylide ligands. *Dyes Pigm.* **2016**, *126*, 165–172. [\[CrossRef\]](#)

41. Lai, S.-W.; Chan, M.C.-W.; Cheung, T.-C.; Peng, S.-M.; Che, C.-M. Probing d^8 - d^8 Interactions in Luminescent Mono- and Binuclear Cyclometalated Platinum(II) Complexes of 6-Phenyl-2,2'-bipyridines. *Inorg. Chem.* **1999**, *38*, 4046–4055. [[CrossRef](#)]
42. Shi, H.; Clarkson, G.J.; Sadler, P.J. Dual action photosensitive platinum(II) anticancer prodrugs with photoreleasable azide ligands. *Inorg. Chim. Acta* **2019**, *489*, 230–235. [[CrossRef](#)]
43. Hobert, S.E.; Carney, J.T.; Cummings, S.D. Synthesis and luminescence properties of platinum(II) complexes of 4'-chloro-2,2':6',2''-terpyridine and 4,4',4''-trichloro-2,2':6',2''-terpyridine. *Inorg. Chim. Acta* **2001**, *318*, 89–96. [[CrossRef](#)]
44. Martínez-Martínez, V.; Llano, R.S.; Furukawa, S.; Takashima, Y.; Arbeloa, I.L.; Kitagawa, S. Enhanced Phosphorescence Emission by Incorporating Aromatic Halides into an Entangled Coordination Framework Based on Naphthalenediimide. *ChemPhysChem* **2014**, *15*, 2517–2521. [[CrossRef](#)]
45. Liu, R.; Li, Y.; Li, Y.; Zhu, H.; Sun, W. Photophysics and Nonlinear Absorption of Cyclometalated 4,6-Diphenyl-2,2'-bipyridyl Platinum(II) Complexes with Different Acetylide Ligands. *J. Phys. Chem. A* **2010**, *114*, 12639–12645. [[CrossRef](#)]
46. Schaffner-Hamann, C.; von Zelewsky, A.; Barbieri, A.; Barigelletti, F.; Muller, G.; Riehl, J.P.; Neels, A. Diastereoselective Formation of Chiral Tris-Cyclometalated Iridium (III) Complexes: Characterization and Photophysical Properties. *J. Am. Chem. Soc.* **2004**, *126*, 9339–9348. [[CrossRef](#)]
47. Murov, S.L.; Carmichael, I.; Hug, G.L. *Handbook of Photochemistry*, 3rd ed.; Taylor & Francis Group: New York, NY, USA, 2006; pp. 424–545.
48. Shafikov, M.Z.; Suleymanova, A.F.; Kutta, R.J.; Brandl, F.; Gorski, A.; Czerwieniec, R. Dual emissive dinuclear Pt(II) complexes and application to singlet oxygen generation. *J. Mater. Chem. C* **2021**, *9*, 5808–5818. [[CrossRef](#)]
49. Abdel-Shafi, A.A.; Beer, P.D.; Mortimera, R.J.; Wilkinson, F. Photosensitized Generation of Singlet Oxygen from (Substituted Bipyridine)ruthenium(II) Complexes. *Helv. Chim. Acta* **2001**, *84*, 2784–2795. [[CrossRef](#)]
50. Abdel-Shafi, A.A.; Bourdelandeb, J.L.; Ali, S.S. Photosensitized generation of singlet oxygen from rhenium(I) and iridium(III) complexes. *Dalton Trans.* **2007**, 2510–2516. [[CrossRef](#)]
51. Kearns, D.R. Physical and chemical properties of singlet molecular oxygen. *Chem. Rev.* **1971**, *71*, 395–427. [[CrossRef](#)]
52. Abdel-Shafi, A.A.; Beer, P.D.; Mortimera, R.J.; Wilkinson, F. Photosensitized generation of singlet oxygen from ruthenium(II)-substituted benzoaza-crown-bipyridine complexes. *Phys. Chem. Chem. Phys.* **2000**, *2*, 3137–3144. [[CrossRef](#)]
53. Ji, Z.; Li, Y.; Sun, W. 4'-(5''-R-Pyrimidyl)-2,2':6',2''-terpyridyl (R = H, OEt, Ph, Cl, CN) Platinum(II) Phenylacetylide Complexes: Synthesis and Photophysics. *Inorg. Chem.* **2008**, *47*, 7599–7607. [[CrossRef](#)] [[PubMed](#)]
54. Lázaro, A.; Cunha, C.; Bosque, R.; Pina, J.; Ward, J.S.; Truong, K.-N.; Rissanen, K.; Lima, J.C.; Crespo, M.; de Melo, J.S.S.; et al. Room-Temperature Phosphorescence and Efficient Singlet Oxygen Production by Cyclometalated Pt(II) Complexes with Aromatic Alkynyl Ligands. *Inorg. Chem.* **2020**, *59*, 8220–8230. [[CrossRef](#)] [[PubMed](#)]
55. Yarnell, J.E.; Chakraborty, A.; Myahkostupov, M.; Wright, K.M.; Castellano, F.N. Long-lived triplet excited state in a platinum(II) perylene monoimide complex. *Dalton Trans.* **2018**, *47*, 15071–15081. [[CrossRef](#)]
56. Lin, H.; Wang, J.; Zhao, J.; Zhuang, Y.; Liu, C.; Zhu, Y.; Jia, H.; Wu, K.; Shen, J.; Fu, X.; et al. Molecular Dipole-Induced Photoredox Catalysis for Hydrogen Evolution over Self-Assembled Naphthalimide Nanoribbons. *Angew. Chem. Int. Ed.* **2022**, *61*, e2021176.
57. Hofmann, A.; Dahlenburg, L.; van Eldik, R. Cyclometalated Analogues of Platinum Terpyridine Complexes: Kinetic Study of the Strong σ -Donor Cis and Trans Effects of Carbon in the Presence of a π -Acceptor Ligand Backbone. *Inorg. Chem.* **2003**, *42*, 6528–6538. [[CrossRef](#)]
58. Laurila, E.; Oresmaa, L.; Niskanen, M.; Hirva, P.; Haukka, M. Metal-Metal Interactions in Stacked Mononuclear and Dinuclear Rhodium 2,20-Biimidazole Carbonyl Complexes. *Cryst. Growth Des.* **2010**, *10*, 3775–3786. [[CrossRef](#)]
59. Mirzaei, S.; Ivanov, M.V.; Timerghazin, Q.K. Improving Performance of the SMD Solvation Model: Bondi Radii Improve Predicted Aqueous Solvation Free Energies of Ions and pKa Values of Thiols. *J. Phys. Chem. A* **2019**, *123*, 9498–9504. [[CrossRef](#)]

Disclaimer/Publisher's Note: The statements, opinions and data contained in all publications are solely those of the individual author(s) and contributor(s) and not of MDPI and/or the editor(s). MDPI and/or the editor(s) disclaim responsibility for any injury to people or property resulting from any ideas, methods, instructions or products referred to in the content.